JOURNAL OF PROPULSION AND POWER
Vol. 19, No. 1, January–February 2003

Mixing Augmentation of Transverse Injection in Scramjet Combustor

Sang-Hyeon Lee*
University of Ulsan, Ulsan 680-749, Republic of Korea
and
Tohru Mitani†
National Aerospace Laboratory, Miyagi 981-1525, Japan

A method for augmenting the mixing of transverse injection in a scramjet combustor is suggested, and its effectiveness is checked by numerical methods. The intent was to promote streamwise vorticity by modifying the injector geometry using a cavity to increase the mixing rate and penetration. A three-dimensional Navier–Stokes code adopting the upwind method of Edwards's low diffusion flux splitting scheme was used. The k–ω SST turbulence model was used to calculate the turbulent viscosity. The injector models proposed showed remarkable increases of streamwise vorticity and, as a result, significant improvements in mixing characteristics such as mixing rate and penetration. However, the proposed models also showed additional losses of stagnation pressure. The mixing characteristics are strongly related to the jet-to-cross flow momentum flux ratio J. In the case of higher values of J, slower mixing rates, higher penetration, and more losses of stagnation pressure are shown.

Nomenclature

D	=	diameter of injector nozzle
J	=	jet-to-cross-flow momentum flux ratio
L_{mix}	=	mixing length
M	=	Mach number
P_0	=	average stagnation pressure
p	=	static pressure
T	=	temperature
W_s	=	molecular weight of species
Y	=	mass-fraction
Z_f	=	penetration distance of fuel jet normalized by D
Γ	=	circulation normalized by u_∞/D
μ, ν	=	viscosity and dynamic viscosity
ρ	=	density

Subscripts

a	=	air
f	=	fuel jet
i	=	condition of air inflow
j	=	condition of jet exit
s	=	species
w	=	wall
0	=	stagnation

Introduction

THE design of a supersonic combustion ramjet (scramjet) combustor requires very efficient fuel–air mixing methods because of the short residence time of airflow within the engine. The residence time of airflow in scramjet engines is only about a millisecond for typical flight conditions. Therefore, rapid mixing between the fuel and air is required, while the stagnation pressure loss and the heat loads must be minimized.[1–5]

One reliable method of fuel injection for a scramjet engine is transverse injection into the airflow because the transverse injection provides rapid fuel–air mixing and rapid penetration of the jet into the airflow. Transverse injection into a supersonic crossflow has been the subject of many experimental and computational studies including mixing, combustion, ignition, and measuring technologies.[3–15] A schematic of a single transverse injection is shown in Fig. 1. There is a three-dimensional bow shock in front of the injection hole. The flowfield of transverse injection into the supersonic crossflow is very complex. There are many shock structures: the bow shock in front of the jet flow, the separation shock generated due to the interaction between the bow shock and boundary layer, the barrel shock, the Mach disk, etc. These shock waves produce significant stagnation pressure losses. A vortex pair is formed along the jet flow mainly due to the expansion flows toward the wake region behind the injection hole, and its evolution is a very complex process involving three dimensional tilting and folding of vortical structures near the jet exit and dominance of the influence of the crossflow farther downstream. It is well known that this vortex pair has an important role in the mixing process. Results of previous studies have shown that the backpressure, pressure around the injection hole, has a close relationship to the structure of shock waves and Mach disk.[7,8,14,15] Therefore, as a result, the backpressure has a significant influence on the flow structure such as the formation and evolution processes of streamwise vorticity.

This study was conducted to find more efficient methods to augment the mixing characteristics of transverse injection. It is well known that streamwise vorticity is one of the key parameters of mixing characteristics such as mixing rate and penetration. Therefore, increasing streamwise vorticity to augment mixing characteristics is often tried with modifications of injector geometry. Based on that one of the main factors controlling the characteristics of the jet flow in transverse injection is the backpressure, attempts have been made to modulate the distribution of the backpressure with modifications of injector geometry to promote streamwise vorticity. This study was motivated by the idea that a reduction of backpressure, especially around the front hemisphere of the injection hole, would be more favorable to increase streamwise vorticity in transverse

Presented as Paper 2000-0090 at the 28th Aerospace Sciences Meeting and Exhibit, Reno, NV, 10–13 January 2000; received 30 January 2002; revision received 6 September 2002; accepted for publication 9 September 2002.

*Assistant Professor, School of Transport Systems Engineering; lsh@uou.ulsan.ac.kr. AIAA Member.

†Head of Ramjet Combustion Group, Kakuda Center, Kimigaya, Kakuda. AIAA Member.

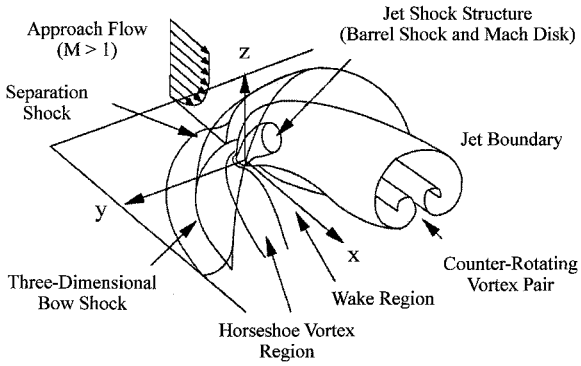

Fig. 1 Perspective view of mean transverse injection flowfield.[15]

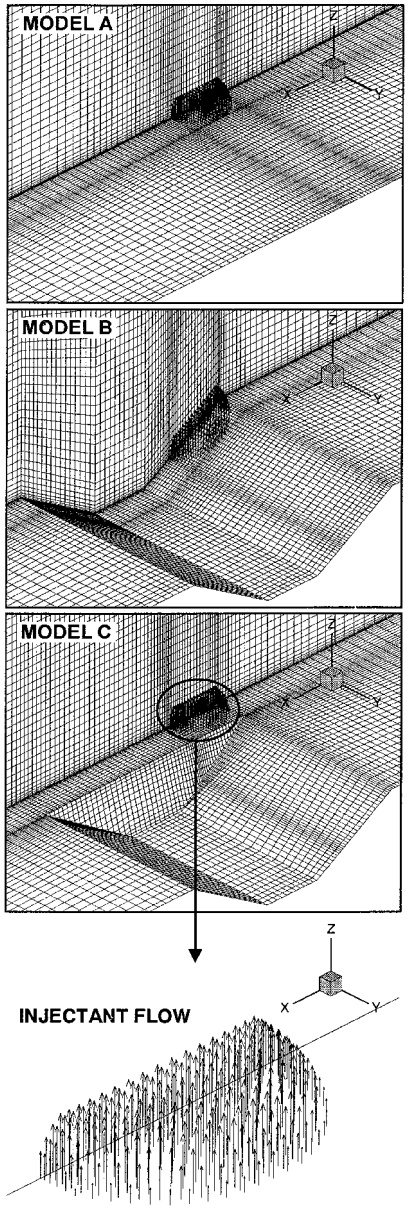

Fig. 2 Grid systems near injection hole and jet flowfield.

injection. To reduce the backpressure around the front hemisphere of the injection hole, some modifications of injector geometry are introduced with cavities around the injection hole. A cavity near the injection hole would reduce the backpressure with the aid of flow expansions generated over the cavity, which would make the crossflow deflect more easily toward the jet flow and, as a result, would favorably increase streamwise vorticity. This concept to augment mixing characteristics was tested with a three-dimensional Navier–Stokes computational code with the k–ω SST turbulence model.

Three kinds of model injectors were tested. The first model shown in Fig. 2 is the canonical model (model A) with no cavity. The second model (model B) is designed to reduce backpressure, especially around the front hemisphere of the injection hole with cavities near the injection hole. The cavity geometry of model B is very simple; there is an expansion ramp, base, and compression wedge in turn. The injection hole is located at the beginning part of the cavity. The last model (model C) is a modification of model B. In a later section, the geometry and grid systems will be discussed in detail. We will show that mixing augmentation is strongly related with streamwise vorticity and the distribution of backpressure around the injection hole. We will also demonstrate that the models B and C improve the mixing characteristics.

The main parameters investigated in the present study are mixing rate, penetration distance, and stagnation pressure loss. The goals of mixing augmentation are a higher mixing rate, a higher penetration distance, and a lower stagnation pressure loss. The mixing rate is one of the most important parameters because an enhancement of the mixing rate directly results in an enhancement of combustion in a scramjet combustor. The penetration distance of the injectant is also an important parameter because the fuel should be far enough away from the combustor wall to enhance its mixing with air and to avoid wall heating in scramjet combustors. An excessive loss of stagnation pressure should be avoided because the loss of stagnation pressure results in a loss of thrust.

Calculations

Governing Equations

Three-dimensional Navier–Stokes equations (see Ref. 16) were used to solve mean flow and the k–ω SST turbulence model[17,18] was used to calculate turbulent viscosity. These governing equations are expressed in vector form with tensor notations:

$$\frac{\partial \boldsymbol{Q}}{\partial t}+\frac{\partial \boldsymbol{E}}{\partial x}+\frac{\partial \boldsymbol{F}}{\partial y}+\frac{\partial \boldsymbol{G}}{\partial z}=\frac{\partial \boldsymbol{E}_v}{\partial x}+\frac{\partial \boldsymbol{F}_v}{\partial y}+\frac{\partial \boldsymbol{G}_v}{\partial z}+\boldsymbol{S}_t \tag{1}$$

$$\boldsymbol{Q}=[\rho_a,\rho_f,\rho u,\rho v,\rho w,\rho e_0,\rho k,\rho\omega]^T \tag{2}$$

$$\boldsymbol{E}=\left[\rho_a u,\rho_f u,\rho u^2+p,\rho uv,\rho uw,\rho h_0 u,\rho ku,\rho\omega u\right]^T \tag{3}$$

$$\boldsymbol{F}=\left[\rho_a v,\rho_f v,\rho vu,\rho v^2+p,\rho vw,\rho h_0 v,\rho kv,\rho\omega v\right]^T \tag{4}$$

$$\boldsymbol{G}=\left[\rho_a w,\rho_f w,\rho wu,\rho wv,\rho w^2+p,\rho h_0 w,\rho kw,\rho\omega w\right]^T \tag{5}$$

$$\boldsymbol{E}_v=\left[\rho_a u_a^d,\rho_f u_f^d,\tau_{xx},\tau_{xy},\tau_{xz},\tau_{xn}u_n-q_x,\mu^k k_{,x},\mu^\omega\omega_{,x}\right]^T \tag{6}$$

$$\boldsymbol{F}_v=\left[\rho_a v_a^d,\rho_f v_f^d,\tau_{yx},\tau_{yy},\tau_{yz},\tau_{yn}u_n-q_y,\mu^k k_{,y},\mu^\omega\omega_{,y}\right]^T \tag{7}$$

$$\boldsymbol{G}_v=\left[\rho_a w_a^d,\rho_f w_f^d,\tau_{zx},\tau_{zy},\tau_{zz},\tau_{zn}u_n-q_z,\mu^k k_{,z},\mu^\omega\omega_{,z}\right]^T \tag{8}$$

$$\boldsymbol{S}_t=[0,0,0,0,0,0,P_k,P_\omega]^T \tag{9}$$

$$\rho=\sum_{s=a,f}\rho_s,\qquad p=\rho\sum_{s=a,f}\frac{Y_s}{W_s}T \tag{10}$$

$$\mu^k=\mu_L+\sigma^*\mu_T,\qquad \mu^\omega=\mu_L+\sigma\mu_T \tag{11}$$

$$\nu_T=\frac{a_1 k}{\max(a_1\omega,\Omega F_2)} \tag{12}$$

$$P_k=\tau_{mn}u_{m,n}-\beta^*\rho\omega k$$

$$P_\omega=\frac{\alpha}{\nu_T\tau_{mn}u_{m,n}}-\beta\rho\omega^2+2\sigma_{\omega 2}\frac{\rho}{\omega}k_{,n}\omega_{,n} \tag{13}$$

where $\boldsymbol{Q}$ is the solution vector; $\boldsymbol{E}$, $\boldsymbol{F}$, and $\boldsymbol{G}$ are the convection vectors; $\boldsymbol{E}_v$, $\boldsymbol{F}_v$, and $\boldsymbol{G}_v$ are viscous vectors; and $\boldsymbol{S}_t$ is a turbulent source vector. The indices L and T denote the laminar and turbulent

properties, respectively. The variables k and ω are turbulent kinetic energy and turbulent dissipation variable, respectively. The turbulence model coefficients σ^*, σ, $\sigma_{\omega 2}$, β^*, β, α, and a_1 are those of the Menter's k–ω SST turbulence model.[17,18] Ω is an absolute value of vorticity, and F_2 is a function of k, ω, and distance from wall. A model for the dilatation–dissipation term suggested by Wilcox[19] is included to predict the compressibility effects. Diffusion velocity of each species is calculated with the Fick's law:

$$Y_s u_s^d = -D_s \frac{\partial Y_s}{\partial x}, \qquad Y_s v_s^d = -D_s \frac{\partial Y_s}{\partial y}, \qquad Y_s w_s^d = -D_s \frac{\partial Y_s}{\partial z} \tag{14}$$

where D_s is diffusivity of s species and $s = a, f$.

The formula and data of viscosity, thermal conductivity, and binary diffusivity are taken from Reid et al.[20] The intermolecular potential function is the Lennard–Jones 12–6 potential. The viscosity of a pure gas is obtained from Chapman–Enskog equation, and the viscosity of a gas mixture is calculated using the Wilke method. The thermal conductivity of a pure gas is obtained from the Eucken method, and the thermal conductivity of gas mixture is calculated with Wassiljewa equation modified by Mason and Saxena. The diffusivity of a binary gas mixture is obtained from Chapman–Enskog equation, and the diffusivity of a gas in the mixture is calculated with Blanc's law. The turbulent diffusivity and turbulent conductivity are obtained from the turbulent viscosity. The turbulent Prandtl number and turbulent Schmidt number are both 0.9.

A finite volume method is used to discretize the Navier–Stokes equations. To the get flux vector at the surface of grid cell, Edwards's low diffusion flux splitting (LDFS) scheme[21] is adopted. The lower–upper symmetric Gauss–Seidel (LU-SGS) scheme (see Ref. 22) is used for time integration.

Geometry of Models and Grid Systems

Figure 2 shows the geometries and grid systems near the injection hole of the model combustors. The length of the cavity is $4.0D$, the expansion angles of the front and rear ramps are both 30 deg. The length of the cavity base is $1.0D$. The jets are injected vertically relative to the freestream. The diameter of the circular injection hole, D, is 3.18 mm (same as that of the Gruber and Goss[15] experiment). The length of the combustor model is $28D$ ($8D$ before and $20D$ after the injection hole), the width is $3.5D$, and the height is $6D$. The center of the injection hole is located at the origin of the coordinate system. The round jet was made with a numerical technique:

$$w_{f,\text{wall}} = f(r)a_j, \qquad f(r) = \begin{cases} 1, & r \le R - \delta \\ \sqrt{R-r}/\sqrt{\delta}, & R - \delta \le r \le R \\ 0, & r > R \end{cases} \tag{15}$$

where $w_{f,\text{wall}}$ is the vertical velocity of the fuel the jet at wall, a_j the sonic speed of the jet, r the distance from center of the injection hole, R the radius of the injection hole, and δ thickness of boundary layer. In the present study, the boundary-layer thickness δ is set as $0.2D$. The grid points were clustered towards the position $|x - x_c| = R$ and $|y - y_c| = R$ to make the cross-sectional shape of the jet be a circular one.

Model A is the canonical injector model with no cavity. The calculation results in model A were compared to the experimental results of Gruber and Goss[15] to validate the computation code used in the present study.

In model B, there is a cavity near the injection hole to reduce the backpressure, especially around the front hemisphere of the injection hole. The cavity geometry of model B is very simple, that is, expansion ramp, base, and compression wedge, respectively. The injection hole in model B is located in the front region of the cavity because the mixing characteristics there were better than any other position according to preliminary studies. The expansion angle of the ramp is 30 deg, and the horizontal length of the expansion ramp is $1.5D$; hence, the depth of the cavity is $0.87D$. The length of cavity base is $1.0D$. The compression angle of the wedge is 30 deg, and the horizontal length of the compression ramp is $1.5D$.

Model C is a modification of model B and has almost the same geometry as model B except in the region before and after the injection hole. The cavity only exists beside the injection hole. Hence, there are no ramps in the front and rear regions of the injection hole and there is a lateral step between the region of the injection hole and the cavity. The injection hole in model C is located in the front region of the step because the mixing characteristics there were better than any other position as indicated in a preliminary study. The geometry of the cavity is the same as model B.

The number of grid points of the primary grid system is $160[x] \times 45[y] \times 55[z]$ (= 396,000). All of the calculations were conducted on the primary grid system. To check grid independence, additional calculations on two different grid systems were conducted. The number of grid points of the second grid system is $125[x] \times 34[y] \times 43[z]$ (= 182,750, 46% of the primary grid system), and the number of grid points of the third grid system is $190[x] \times 56[y] \times 67[z]$ (= 712,880 (180% of the primary grid system). The grid points are clustered near the walls and near the injection hole and wall boundary.

Flow Conditions and Boundary Conditions

The calculation conditions are the same as the experimental conditions of Gruber and Goss[15] for the purpose of comparing the results of this study. In the experiment, the injectant was air. The inflow air and injectant are treated as ideal gases. The Mach numbers of the airflow and the jet flow are 1.95 and 1.0, respectively. The jet is injected vertically. The stagnation pressure and stagnation temperature of the air inflow are 317.7 kPa and 297 K, respectively. The penetration and mixing rate of the jet are controlled by the jet-to-cross flow momentum flux ratio J, defined as

$$J \equiv \frac{(\rho V^2)_f}{(\rho V^2)_a} = \frac{(\gamma p M^2)_f}{(\gamma p M^2)_a} \tag{16}$$

In this paper, a parametric study was conducted with a variation of the value of J from 0.5 to 2.0. The stagnation temperature of the injectant is 297 K, and the static pressure and density at the nozzle exit are determined according to the value of J.

Calculations were conducted on the half-domain divided by the symmetric surface of the injection hole to reduce the computation time. The top surface and right surface of computational domain were treated as open boundaries. The boundary conditions of the turbulence model for solid walls are

$$k = 0, \qquad \omega = 10\frac{6\nu}{\beta_1^*(\Delta y_1)^2} \tag{17}$$

where Δy_1 is the distance between wall and the first grid point away from the wall. The turbulent viscosities of the inflow and the jet flow are both 0.01 times the laminar viscosity of the inflow air.

Results

Code Validation

To validate the code used, the results of the present study are compared with the experimental results of Gruber and Goss.[15] Also, the calculations on two different grid systems were conducted to check grid independence. Figure 3a shows a comparison of the distributions of the wall pressure along the centerline ($y = 0$). The center of the injection hole is located at $(x, y) = (0, 0)$. Figure 3b shows a comparison of the distributions of backpressure around the injection hole. The position −90 deg denotes the front of the injection hole, and the position 90 deg denotes the rear end of the injection hole. The radial distance between the measuring point and the boundary of the injection hole is $0.2D$.

Even the calculation on the second grid system (the number of grid points is about 46% of the primary grid system) showed reasonable agreement with the results of Gruber and Goss[15]; the largest difference occurs at $x/D = -1.6$ by 9.2% of the experimental datum. The calculation on the third grid system (the number of grid

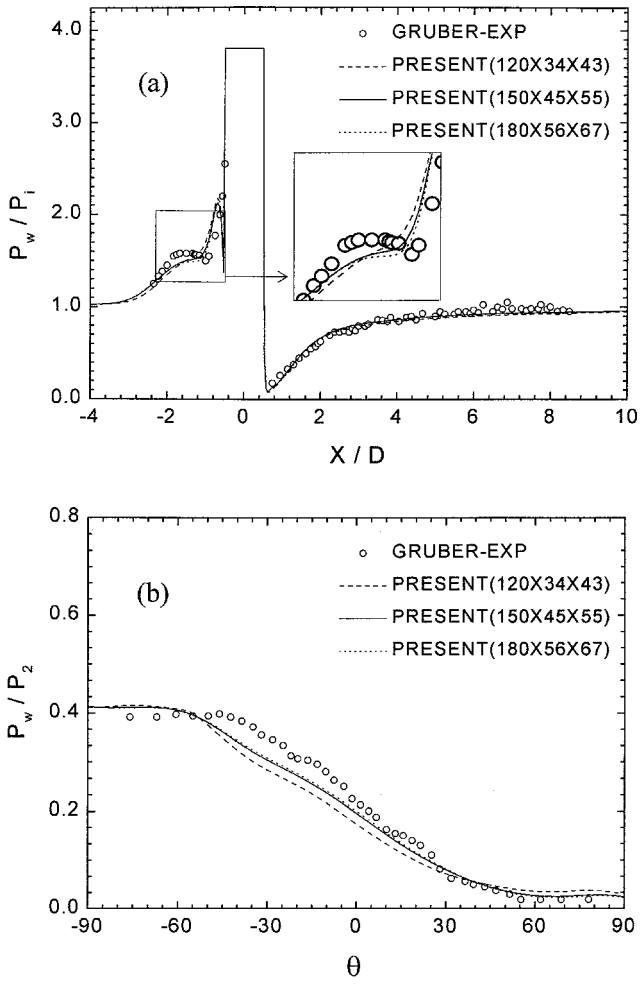

Fig. 3 Validation results in model A (J = 1.0): a) centerline wall pressure profile and b) distribution of backpressure.

points is about 180% of the primary grid system) showed almost the same results as the primary grid system; the largest difference occurs at $x/D = -1.0$ by 2.7% of the datum of primary grid system. The wall pressures along the center axis in the present study showed almost the same results as the experimental results of Gruber and Goss[15] except for a small region in front of the injection hole. Backpressures around the injection hole in the present study have slightly lower values beside the injection hole (between −45 and 30 deg) than that of the experimental results of Gruber and Goss[15]; the largest difference occurs at the −42-deg position by 9.5% of the experimental datum.

Global View of Mixing Process

To compare the overall trends of the mixing process among the three models, the mass fractions of injectant are plotted in Fig. 4. Figure 4a shows the mixing process when the value of the jet-to-crossflow momentum flux ratio J is 0.5, Figs. 4b and 4c show the mixing processes when the values of J are 1.0 and 2.0, respectively. The first part of Figs. 4a–4c shows the mixing process of the model A, second and third parts show the mixing processes of models B and C, respectively.

A comparison among Figs. 4 in each row illustrates that the mixing rates and the penetration distances of injectants in models B and C are higher than those of model A. As such, two models proposed in this study show different trends of mixing enhancement. At the near fields, model B strongly enhances the mixing rate, whereas model C only slightly enhances the mixing rate. However, at the far fields, model B slightly enhances the mixing rate, whereas model C strongly enhances the mixing rate. In a global sense, models B and C both show an enhancement of penetration. In the following sections, the reason and the measure of mixing enhancement in models B and C will be discussed.

A comparison of Figs. 4a–4c illustrates that the mixing rate decreases and the penetration distance of the injectant increases as the value of J increases. This suggests that the value of J should be carefully selected for a scramjet combustor because the mixing rate and penetration distance of the injectant show opposite trends from each other with a variance in the value of J.

Flowfields Near Injection Hole

The pressure fields and velocity fields in the x-directional cross sections near the injection hole are plotted in Fig. 5 to understand the formation and evolution processes of streamwise vorticities. The value of J is 1.0. In the pressure fields, the dark region has high pressure, and the bright region has low pressure. The highest value of pressure is $1.4p_i$, and the lowest value is $0.1p_i$. In the velocity fields, the size of the velocity vector shown is the velocity magnitude of inflow air.

At the planes $x/D = 0.5$, the pressure fields of three models show the existence of bow shocks. The bulk sizes of the high-pressure regions of models A and C are nearly identical, whereas the bulk size of the high-pressure region of model B is much smaller. This is because there is an expansion ramp behind the injection hole in model B unlike the other models. In the velocity fields, models B and C show much stronger expansion flows in the lateral direction than model A.

The successive parts of Fig. 5 from the planes $x/D = 1.0$ to the planes $x/D = 3.0$ show the formation and evolution processes of streamwise vorticities in the three models. Note that in models B and C much larger and stronger vortex flows are generated than in model A between the planes $x/D = 1.0$ and the planes $x/D = 3.0$. The pressure fields show that these vortex flows are generated due to the pressure gradients formed in the cavity regions. The shapes of the vortex flows of models B and C are slightly different from each other, which is due to the existence of a lateral step in model C.

At the planes $x/D = 4.0$, models B and C still have larger vortex flows and stronger vorticities than model A. These trends would be maintained downstream because the strong pressure gradients disappear downstream. From the preceding description, it may be stated that models B and C have higher streamwise vorticities than model A.

Streamwise Vorticity

It is well known that streamwise vorticity can greatly influence the mixing process in high-speed flows.[23–27] Streamwise vorticity produces a large convection flow in the plane perpendicular to the streamwise direction and promotes mixing between air and injectants. The transverse injection across the supersonic flow also produces a strong vortex along the jet flow. Therefore, there must be strong influences of streamwise vorticity on mixing characteristics. To understand the influences of streamwise vorticity on mixing rate, penetration and changes of circulation in the y–z plane are analyzed. The definition of normalized circulation is expressed in the following form:

$$\Gamma(x) = \iint_{y,z} \left| \frac{\partial v}{\partial z} - \frac{\partial w}{\partial y} \right| \rho u \, dy \, dz \tag{18}$$

The histories of circulation of all models are plotted in Fig. 6. The streamwise vorticities produced using models B and C are higher, in general, than what is produced using model A. These higher circulations in models B and C are due to the vorticities generated by the cavity regions $x/D = 1.0$ and 2.0. As already, mentioned, in models B and C much larger and stronger vortex flows are generated between the planes $x/D = 1.0$ and the planes $x/D = 3.0$ due to the pressure gradients formed in the cavity region. The higher second peak of circulation in model C is believed to be due to vortex stretching with the aid of the lateral step of model C (Fig. 5).

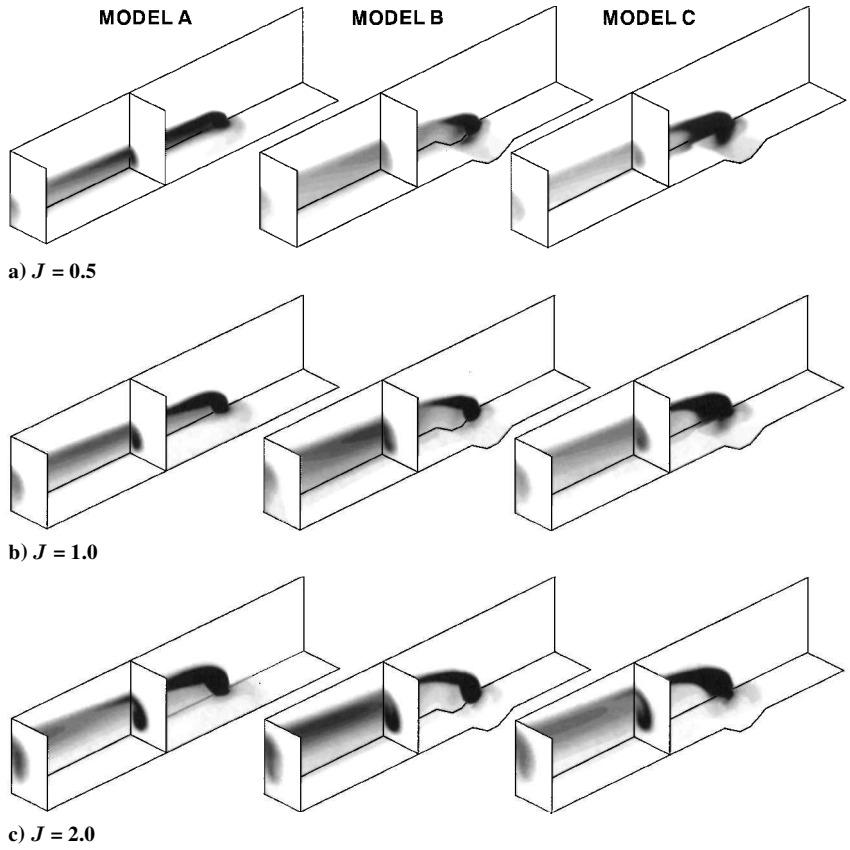

Fig. 4 Overall view of mixing process: injectant mass fraction of model A in the first column, of model B in the second column, and of model C in the third column; darker region has higher mass fraction, and highest value of mass fraction is 1.0.

The strength of circulation is closely related to the value of J (jet-to-crossflow momentum flux ratio). In the case of a higher value of J, there is stronger streamwise vorticity than that with a lower value of J. This is believed to be because a jet flow with a higher value of J more strongly interacts with the airflow. Another possible reason is that an injectant with a larger value of J has larger density, which produces stronger baroclinic sources.[23–25]

Backpressure

It is believed that backpressure strongly influences the characteristics of jet flows. The trends of backpressure in our three models are plotted in Fig. 7 to obtain information about the relationship between pressure distribution and streamwise vorticity. The measuring points are $0.2D$ away from the boundary of the injection hole. The −90-deg position is the front of the hole and the 90-deg position is the rear end of the hole. Backpressures are normalized by the pressure p_2, which is the pressure of airflow behind a normal shock wave.[15]

Models B and C have lower backpressures around the front hemisphere and higher backpressures around the rear hemisphere of the injection hole than model A at all values of J. As shown in Fig. 5, these lower backpressures around the front hemisphere in models B and C are the result of flow expansions toward the cavities. The Higher backpressures around the rear hemisphere of models B and C of the injection hole are because the vortex flows induced in the cavities supplement flows toward the wake regions behind the injection hole. A comparison between models B and C shows that model C has lower backpressure around the front hemisphere of the injection hole than model B, which means that the flow expansion toward the cavity in model C is stronger than that in model B. This is consistent with results shown in Fig. 6 that model C has higher streamwise vorticity than model B.

Note that an effective backpressure[7,8,14,15] is not the key parameter to explain mixing augmentation. For instance, among the cases whose values of J are 0.5 (Fig. 7a), models B and C whose effective backpressures are higher that that of model A have a higher mixing rate and higher penetration. This means that the distribution of backpressure is not directly related to the mixing characteristics, but, rather, is strongly related with a formation of streamwise vorticity. Therefore, it can be stated that lower backpressure around the front hemisphere and higher backpressures around the rear hemisphere of the injection hole is more favorable to the generation of streamwise vorticity and, as a result, to the mixing process.

Mixing Rate

The mixing rate is one of the most important parameters of mixing characteristics because the combustion process strongly depends on the mixing process. Figure 8 shows the trends of mixing rates in the models A, B, and C with a variation of the value of J. The definition of mixing rate is the decay rate of maximum injectant mass fraction. The decay rate of the maximum mass fraction of the injectant jet was changed to be almost linear on a log–log scale at the far field (after about $x/D = 8$ in model A). This is believed to be because the mixing process largely depends not on the convection but on mass diffusion at the far fields. Therefore, there is a transition of mixing regime from a convection-dominated regime to a diffusion-dominated regime because there are no flow-acceleration mechanisms at the far field.[23,24]

Models B and C show a higher mixing rate than model A at all values of J. Model B shows the highest mixing rate at the near field, whereas model C shows the highest mixing rate downstream. When it is considered that the streamwise vorticities of models B and C are higher than that of model A (Fig. 6), a stronger streamwise vorticity seems to be the main reason for the enhancement of the mixing rate. This result is consistent with the results of previous studies.[23–27] As mentioned earlier, in Fig. 5 stronger streamwise vorticities in models B and C are believed to be due to additional vorticity generated with the aid of the cavities. The flows expand toward the cavity and turn back to the jet flow, which help the jet to mix with air and to penetrate into the crossflow. From this, it can be stated that models B and C may be more favorable than the canonical model for the mixing process in a real scramjet combustor.

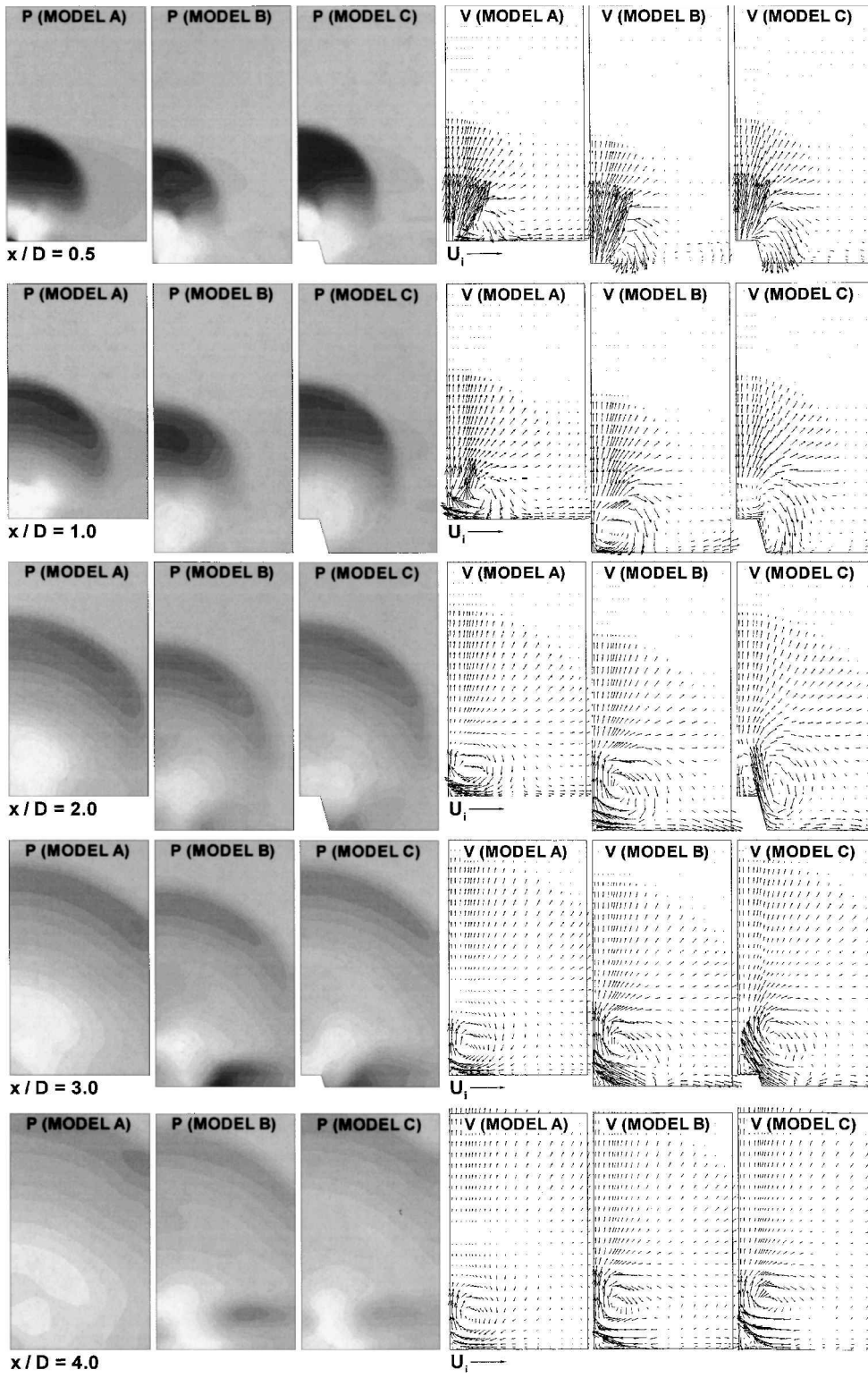

Fig. 5 Comparisons of pressure fields and velocity fields among models A, B, and C at near fields; darker region has higher pressure, and highest pressure is about $3.8p_i$.

Mixing rates are closely related to the value of J. In cases of a higher value of J, slower mixing than that with lower values of J are shown, which because, in cases with a small value of J, there is a weak inertia force of the jet flow. The airflow can disturb or stir more easily the jet flow with a lower value of J than that with a higher value of J. When the variations of streamwise vorticity due to the change of the value of J (Fig. 6) are considered, the streamwise vorticity is not the only parameter for mixing rate; the case with higher value of J has a higher circulation but a lower mixing rate than that with a small value of J. The mixing rate is determined by the streamwise vorticity and the inertia force of the jet flow relative to that of crossflow simultaneously.

The concept of mixing length has been adopted to quantify the mixing capabilities of the three models. The mixing length is evaluated by the downstream distance at which the maximum mass fraction has decayed to 0.5. Figure 9 shows the comparison of the mixing length in the three models. Models B and C have shorter mixing lengths than that of model A, which means that models B and C have higher mixing capabilities than model A. The mixing lengths of all models increased almost linearly with an increase in

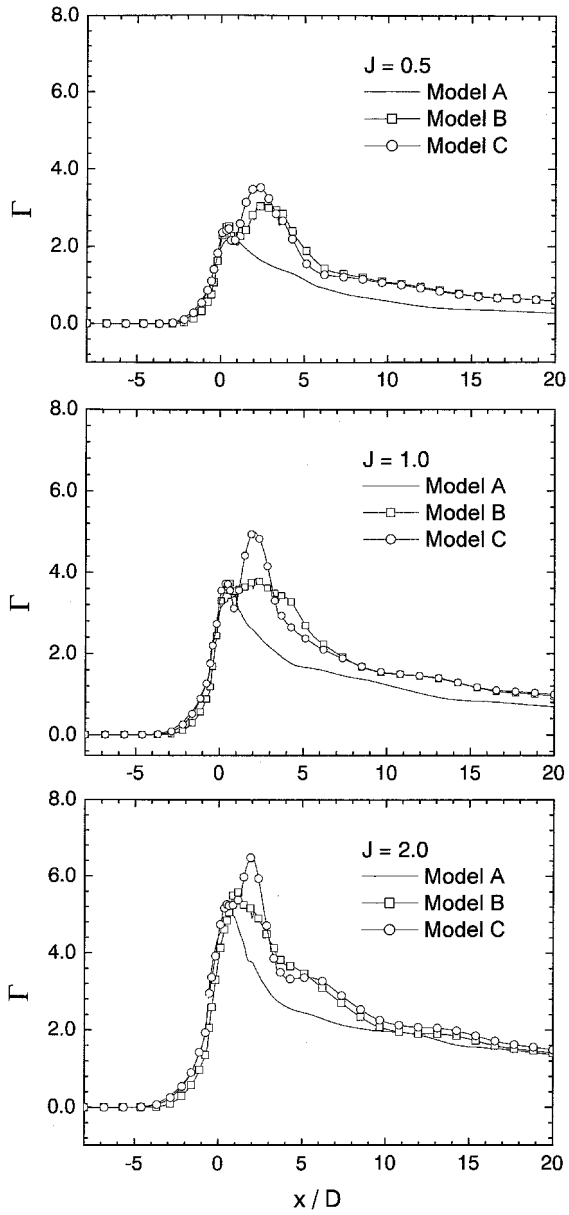

Fig. 6 Comparison of circulation normalized by diameter of injection hole and velocity of inflow air.

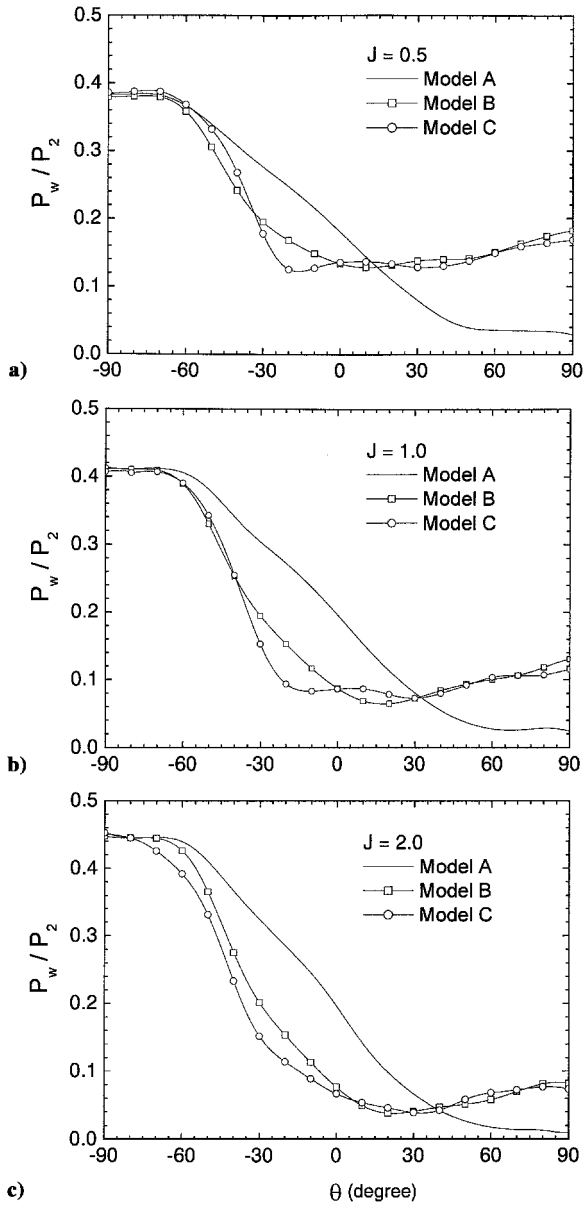

Fig. 7 Distribution of backpressure around injection hole.

the value of J. The increased rates of mixing length of models A and C according to an increase in the value of J are almost the same as each other, whereas the increased rates of the mixing length of model B is higher than those of both models A and C. Therefore, it can be stated that model C would enhance mixing irrespective of the value of J, even if the value of J is up slightly higher than 2.0.

Penetration

The injected fuel must penetrate high enough into the crossflow to minimize wall heating and to maximize combustion efficiency. The penetration distance is estimated with the center of mass of the fuel from the lower wall, which is defined in the following form:

$$Z_f(x) = \iint_{y,z} \rho_f z \, dy \, dz \Big/ \iint_{y,z} \rho_f \, dy \, dz \qquad (19)$$

Figure 10 shows the trajectory of penetration distances of the combustor models. The reference location $z = 0$ is the lower wall of the combustor, not the injection hole, and is the same for all geometries. In every case, the penetration distance increases rapidly right after the injection, but the increasing rate of penetration decreases gradually and finally becomes a constant at the far field.

Models B and C show higher penetration distances than model A at all values of J. The lower penetration of models B and C at the near fields are due to the portions of injectant in the cavity transported by the expansion flows toward the cavities. The rate of penetration increase downstream in model C is almost the same as that in model A, and the rate of penetration increase in model B is slightly higher than that in the other models. The reason why the penetration in model B is lower than that of model C is that the position of the injection hole is lower than that of model C. From this, it can be stated that models B and C are more favorable than the canonical model for combustion in real scramjet combustors.

The penetration distances are closely related with the value of J (jet-to-crossflow momentum flux ratio). In the case of a higher value of J higher penetration distance than that with a lower value of J is shown. This is because jet flow with a higher value of J has a stronger inertia force relative to the crossflow than that with a lower value of J. When only the penetration of the jet is considered, the cases with a higher value of J are more favorable. However, as already mentioned, the tradeoff of mixing rate should be considered.

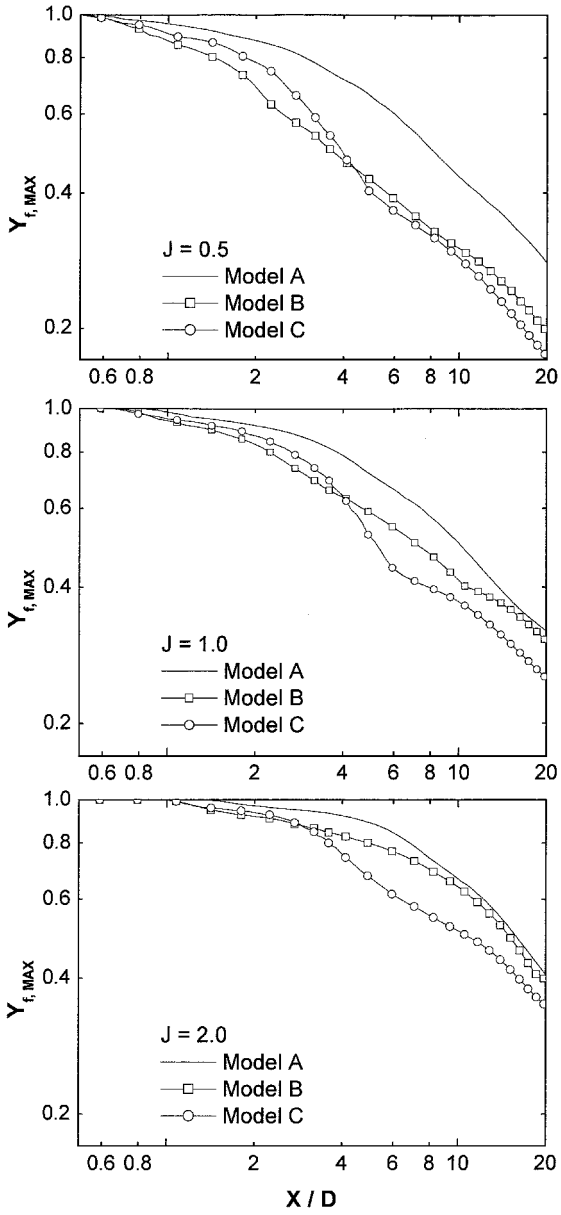

Fig. 8 Comparison of mixing rate expressed by decay rate of maximum mass fraction of injectant (plotted on log–log scale).

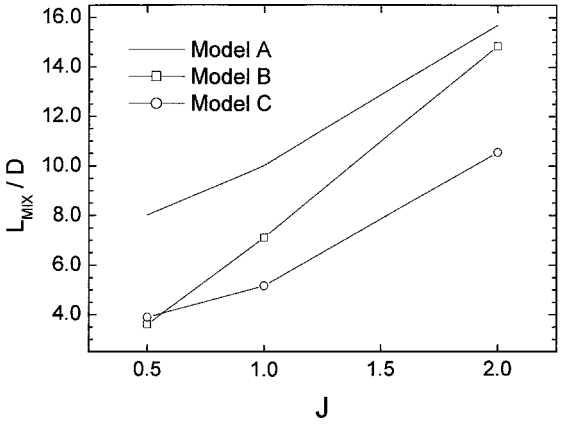

Fig. 9 Comparison of mixing length normalized by diameter of injection hole; mixing length evaluated by downstream distance at which the maximum mass fraction has decayed to 0.5.

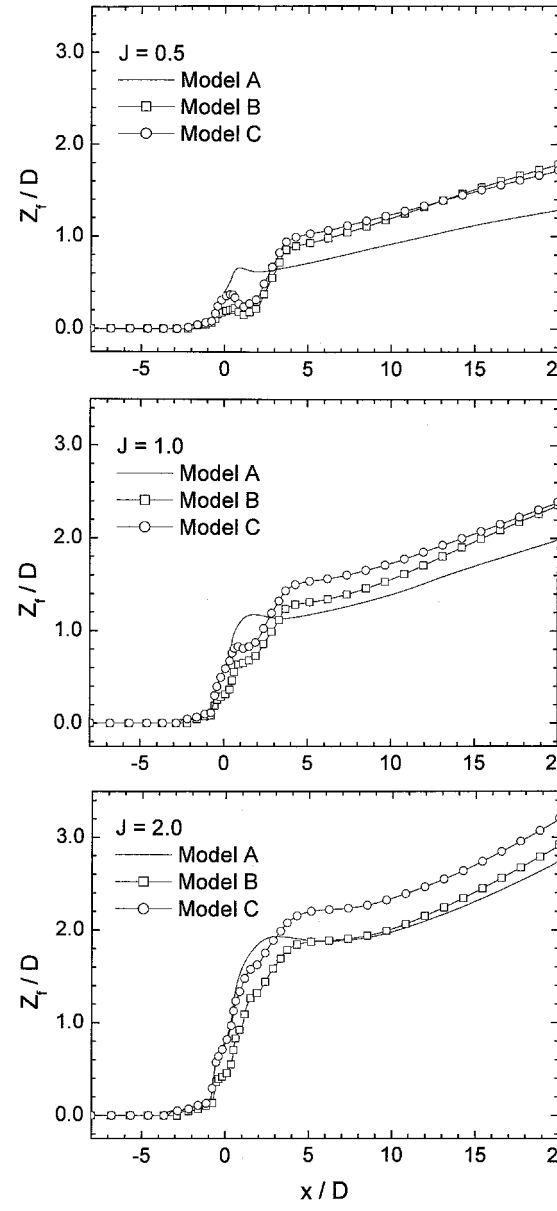

Fig. 10 Comparison of penetration distance normalized by diameter of injection hole.

Stagnation Pressure Loss

Generally, the mixing process produces a loss of stagnation pressure that results in a loss of thrust. Therefore, it should be checked whether or not there are additional losses of stagnation pressure due to mixing augmentation. The definition of average stagnation pressure in the y–z plane is expressed in the following form:

$$P_0(x) = \iint_{y,z} p_0 \rho u \, \mathrm{d}y \, \mathrm{d}z \Big/ \iint_{y,z} \rho u \, \mathrm{d}y \, \mathrm{d}z \tag{20}$$

The stagnation pressure and stagnation temperature are calculated with the thermodynamic relationship:

$$\ln\left(\frac{p_0}{p}\right) = \frac{1}{R}\int_T^{T_0} \frac{c_p}{T}\,\mathrm{d}T$$

$$\int_0^{T_0} c_p \,\mathrm{d}T = \int_0^{T} c_p \,\mathrm{d}T + \frac{1}{2}(u^2 + v^2 + w^2) \tag{21}$$

where c_p is the constant pressure specific heat and R is the gas constant.

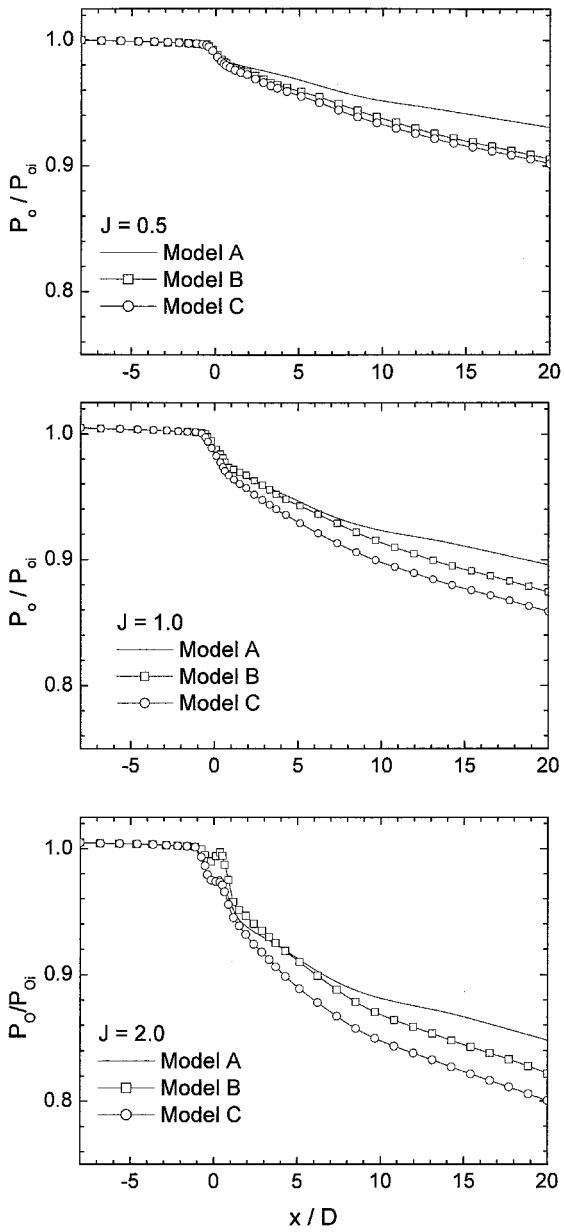

Fig. 11 Comparison of stagnation pressure normalized by stagnation pressure of inflow air.

Figure 11 shows the histories of average stagnation pressure along the streamwise direction in models A, B, and C normalized by the stagnation pressure at inflow. All models show very similar histories of stagnation pressures; there are slow decreases of stagnation pressure in the region before the injection hole ($x = 0$), but the stagnation pressures begin to decrease very steeply from the region right before the injection hole. These rapid decreases of stagnation pressure are believed to be due to bow shock and separation shock formed in front of the jet flows. The decreases of stagnation pressure after the injection are believed to be because of streamwise vortex pair and dissipation. The rates of stagnation pressure loss are reduced after injection due to the supplements of stagnation pressure by the jet flows.

Models B and C show more stagnation pressure losses than model A. These additional losses of stagnation pressures in models B and C occur during the promotions of streamwise vorticity, which agrees well with the Crocco's theorem; in models B and C, the additional streamwise vorticity (shown in Fig. 5) coincides with the additional stagnation pressure loss. When only the stagnation pressure loss is considered, models B and C are unfavorable. However, an enhancement of the mixing rate would enhance the burning rate in a real scramjet combustor and, as a result, increase thrust. Therefore, studies including the burning process should be conducted determine whether or not the mixing augmentation is favorable to the thrust.

Stagnation pressure losses are strongly related to the value of J. The case of a higher value of J shows more loss of stagnation pressure. An increase of stagnation pressure loss with the increase of the value of J is due to two reasons: 1) The case of a higher value of J produces stronger shock waves and, as a result, shows more stagnation pressure loss (compare the decay rates right before the injection hole). 2) The case of a higher value of J produces stronger streamwise vorticity, which was mentioned earlier in the preceding paragraph.

Conclusions

In the present study, a method for the mixing augmentation of the transverse injection in a scramjet combustor was proposed, and its effectiveness was studied using numerical methods. It was intended to promote streamwise vorticity by a modification of the injector geometry with a cavity to increase the mixing rate and penetration.

The injector models proposed in the present study, especially model C, showed significant improvements in the mixing characteristics, such as mixing rate and penetration of the jet. We have also shown that these mixing augmentations are a result of additional productions of streamwise vorticity induced by a cavity. However, the mixing augmentations resulted in an additional loss of stagnation pressure. Therefore, studies including the burning process should be conducted to determine whether or not the mixing augmentation is favorable to the thrust.

Mixing characteristics are strongly related to the jet-to-crossflow momentum flux ratio J. In the case of a higher value of J, a slower mixing rate, higher penetration, and more losses of stagnation pressure are shown.

Acknowledgment

This work was supported by Grant R01-2000-000-00316-0 from the Basic Research Program of the Korea Science and Engineering Foundation.

References

[1]Billig, F. S., "Research on Supersonic Combustion," *Journal of Propulsion and Power*, Vol. 9, No. 4, 1993, pp. 499–514.

[2]Bogdanoff, D. W., "Advanced Injection and Mixing Techniques for Scramjet Combustors," *Journal of Propulsion and Power*, Vol. 10, No. 2, 1994, pp. 183–190.

[3]Bushnell, D. M., "Hypervelocity Scramjet Mixing Enhancement," *Journal of Propulsion and Power*, Vol. 11. No. 5, 1995, pp. 1088–1090.

[4]Northam, G. B., and Anderson, G. Y., "Supersonic Combustion Ramjet Research at Langley," AIAA Paper 86-0159, Jan. 1986.

[5]Schetz, J. A., and Billig, F. S., "Studies of Scramjet Flowfields," AIAA Paper 87-2161, July 1987.

[6]Zukoski, E. E., and Spaid, F. W., "Secondary Injection of Gases into a Supersonic Flow," *AIAA Journal*, Vol. 2, No. 10, 1964, pp. 1689–1696.

[7]Schetz, J. A., Hawkins, P. F., and Lehman, H., "Penetration of Gaseous Jets Injected into a Supersonic Stream," *AIAA Journal*, Vol. 3, No. 11, 1966, pp. 1658–1665.

[8]Billig, F. S., Orth, R. C., and Lasky, M., "A Unified Analysis of Gaseous Jet Penetration," *AIAA Journal*, Vol. 9, No. 6, 1971, pp. 1048–1058.

[9]Spaid, F. W., and Zukoski, E. E., "Further Experiments Concerning Secondary Injection of Gases into a Supersonic Flow," *AIAA Journal*, Vol. 4, No. 12, 1966, pp. 2216–2218.

[10]Papamoschou, D., and Hubbard, D. G., "Visual Observations of Supersonic Transverse Jet," *Experiments in Fluids*, Vol. 14, No. 6, 1993, pp. 468–476.

[11]Abbitt, J. D., III, Segal, C., McDaniel, J. C., Krauss, R. H., and Whitehurst, R. B., "Experimental Supersonic Hydrogen Combustion Employing Staged Injection Behind a Rearward-Facing Step," *Journal of Propulsion and Power*, Vol. 9, No. 4, 1993, pp. 472–478.

[12]Karagozian, A. R., Wang, K. C., Le, A. T., and Smith, O. I., "Transverse Gas Jet Injection Behind a Rearward-Facing Step," *Journal of Propulsion and Power*, Vol. 12, No. 6, 1996, pp. 1129–1136.

[13]Wang, K. C., Smith, O. I., and Karagozian, A. R., "In-Flight Imaging of Transverse Gas Jet Injected into Compressible Crossflows," *AIAA Journal*, Vol. 33, No. 12, 1995, pp. 2259–2263.

[14]Everette, D. E., and Morris, M. J., "Wall Pressure Measurements for a Jet Injected Transversally into a Supersonic Crossflow," *Journal of Propulsion and Power*, Vol. 14. No. 6, 1998, pp. 861–868.

[15]Gruber, M. R., and Goss, L. P., "Surface Pressure Measurements in Supersonic Transverse Injection Flowfields," *Journal of Propulsion and Power*, Vol. 15, No. 5, 1999, pp. 633–641.

[16]Hoffmann, K. A., *Computational Fluid Dynamics for Engineers*, Engineering Education System, Austin, TX, 1989, pp. 306–369.

[17]Menter, F. R., "Two-Equation Eddy-Viscosity Turbulence Models for Engineering Applications," *AIAA Journal*, Vol. 32, No. 8, 1994, pp. 1598–1605.

[18]Menter, F. R., and Rumsey, C. L., "Assessment of Two-Equation Turbulence Models for Transonic Flows," AIAA Paper 94-2343, July 1994.

[19]Wilcox, D. C., *Turbulence Modeling for CFD*, DCW Industries, La Canada, CA, 1993, pp. 73–212.

[20]Reid, C. R., Prausnitz, J. M., and Poling, B. E., *The Properties of Gases and Liquids*, 4th ed., McGraw–Hill, New York, 1988.

[21]Edwards, J. R., "A Low-Diffusion Flux-Splitting Scheme for Navier–Stokes Calculations," *Computers and Fluids*, Vol. 26, No. 6, 1997, pp. 635–659.

[22]Yoon, S., and Jameson, A., "Lower–Upper Symmetric Gauss–Seidel Method for the Euler and Navier–Stokes Equation," *AIAA Journal*, Vol. 26, No. 9, 1988, pp. 1025, 1026.

[23]Lee, S.-H., Jeung, I.-S., and Yoon, Y., "Computational Investigation of Shock-Enhanced Mixing and Combustion," *AIAA Journal*, Vol. 35, No. 12, 1997, pp. 1813–1820.

[24]Lee, S.-H., Jeung, I.-S., and Yoon, Y., "Computational Investigation of Shock-Enhanced Mixing: Application to Circular Cross-Section Combustor," *AIAA Journal*, Vol. 36, No. 11, 1998, pp. 2055–2062.

[25]Waitz, I. A., Marble, F. E., and Zukoski, E. E., "Investigation of a Contoured Wall Injector for Hypervelocity Mixing Augmentation," *AIAA Journal*, Vol. 31, No. 6, 1993, pp. 1014–1021.

[26]Green, S. I., *Fluid Vorticity*, Kluwer Academic, Norwell, MA, 1995, pp. 471–532.

[27]Ton, V. T., Karagozian, A. R., Marble, F. E., Osher, S. J., and Engquist, B. E., "Numerical Simulations of High-Speed Chemically Reacting Flow," *Theoretical and Computational Fluid Dynamics*, Vol. 6, 1994, pp. 161–179.